Available online at www.sciencedirect.com
SCIENCE DIRECT®
Journal of Colloid and Interface Science 260 (2003) 385–397
JOURNAL OF Colloid and Interface Science
www.elsevier.com/locate/jcis

Three-phase capillary entry conditions in pores of noncircular cross-section

M.I.J. van Dijke * and K.S. Sorbie

Institute of Petroleum Engineering, Heriot-Watt University, Riccarton, Edinburgh EH14 4AS, Scotland, United Kingdom

Received 17 May 2002; accepted 19 December 2002

Abstract

In this work we challenge the assumption that the capillary entry pressures for displacements in three-phase flow are the same as those in two-phase flow. Using an energy balance, as derived by R.P. Mayer and R.A. Stowe (J. Colloid Interface Sci. 20 (1965) 893–911) and H.M. Princen (J. Colloid Interface Sci. 30 (1969) 69–75; 30 (1969) 359–371; 34 (1970) 171–184) for two-phase flow, we derive a general formula for determination of the capillary entry pressures for piston-like displacement of two bulk phases in a pore where a third phase may also be present. The method applies to capillaries of angular cross-section and uniform but arbitrary wettability. To use this method we have determined all possible underlying phase occupancies in cross-sections on either side of the main terminal meniscus, in particular the presence of corner arc menisci (AMs). Indeed, the capillary entry pressures for piston-like displacements depend on the pressure in the remaining third phase if the cross-sectional fluid configurations contain this phase. This dependence only vanishes when layers of the intermediate-wetting phase completely separate the wetting and the non-wetting phases. The complexity of the corresponding equations and the quantitative effects are studied using two different geometries, the equilateral triangle and the rhombus. The main difference is that the latter geometry has unequal corners, which may carry different AMs. We have carried out a limited sensitivity study with respect to the effect of wettability, the spreading coefficient of the intermediate-wetting phase, and the aspect ratio of the principal radii of the rhombus.

Keywords: Three-phase; Pore; Angular cross-section; Capillary pressure; Entry condition; Contact angle; Wetting film; Intermediate-wetting layer

1. Introduction

Many studies show that the wetting phase is often present in the corners and roughness of pores (see, e.g., [1]), even if the bulk of the pore is occupied by a different phase. In two-phase flow we may have a non-wetting bulk phase with the wetting phase in corners, while in three-phase flow both the non-wetting and the intermediate-wetting phase may be present in the bulk of the pore [2,3]. For the latter, the intermediate-wetting phase may be present as a layer that separates the wetting and the non-wetting phases even under nonspreading conditions [2,4].

For two-phase flow the possible fluid configurations and the corresponding capillary entry pressures for piston-like displacement in pores with various geometries have been worked out by a number of researchers. The original method was derived by Mayer and Stowe [5] and Princen [6–8] and is therefore called the MS-P method. This powerful method equates the virtual work carried out by the main meniscus between the two phases and the change of surface free energy related to the corner fluid–fluid menisci and fluid–solid contacts. The approach was later applied to different pore cross-sectional geometries, non-zero contact angles, and contact angle hysteresis within a single pore [9–14]. For three-phase flow the fluid configurations have been calculated for various geometries, mainly for the sake of determining volumes and effective conductances (see, e.g., [14,15]), depending on the actual pressure differences, hence radii of curvatures of the fluid–fluid menisci. These configurations may be complicated by the presence of a layer of the intermediate-wetting phase. Necessary conditions for the existence of such layers in corners have been derived by Fenwick and Blunt [2] and Firincioglu et al. [16], although some argue that these layers may not exist for realistic pressure combinations [17].

However, so far true three-phase capillary entry conditions for piston-like displacement have never been consid-

* Corresponding author.
E-mail address: rink@pet.hw.ac.uk (M.I.J. van Dijke).

0021-9797/03/$ – see front matter
doi:10.1016/S0021-9797(02)00228-X

ered. In pore-scale modeling of three-phase flow it is commonly assumed that three-phase displacements can always be described as combinations of two-phase displacements. More specifically, the capillary entry pressures for displacements in three-phase flow are assumed to be the same as those in two-phase flow [18–25], hence calculation of two-phase capillary entry pressures would be sufficient.

In this work we challenge this assumption, supported by observations in the micromodel experiments carried out by Sohrabi et al. [26,27]. In these experiments, displacements between two bulk phases take place in the presence of a corner film of the third phase, which can have different thicknesses, i.e., different pressures. To calculate the capillary entry pressures for piston-like displacement of two phases in the presence of the remaining third phase, we extend the MS-P method to three-phase flow. Thus, we formulate the balance of virtual work and change of surface free energy for a small displacement of a truly three-phase fluid configuration at capillary equilibrium in a single pore of angular cross-section. We allow arbitrary values of the contact angles, but assume that these are constant throughout the pore. Extensions to nonuniformly wetted pores and contact angle hysteresis can then easily be made based on the available work in two-phase flow [12,13].

In Section 2.1, we first determine which fluid configurations are possible, including layers of the intermediate-wetting phase. Section 2.2 describes the actual derivation and provides a general formula for calculating the radii of curvatures, hence capillary entry pressures. Additionally, we indicate under which conditions the resulting pressures are allowed. In Section 3 we apply this formula to the specific cross-sectional geometries of an equilateral triangle and a rhombus, where the latter has the complication of different sized corners and hence different corner fluid occupancies. As such, the rhomboidal tube can be used as a model pore in network models, where it is important to simulate the variation of corner wetting films as a function of the pressure in these films, while the corresponding three-phase capillary entry pressures can still be calculated explicitly.

2. Derivation of capillary entry pressures

2.1. Three-phase fluid configurations

To determine the capillary entry pressures for piston-like displacement in a three-phase system (say water–oil–gas), we first analyze the possible phase occupancies of a single pore. We assume that the pore is a capillary with polygonal cross-section; i.e., individual corners as sketched in Fig. 1 can be distinguished with corner half angle $\gamma \leqslant \pi/2$. At capillary equilibrium the pore cross-section may be occupied by one, two, or all three phases, numbered as 1, non-wetting; 2, intermediate-wetting; and 3, wetting. The wetting order is determined by the respective contact angles θ_{ij}, $ij = 12, 13, 23$, measured through phase j, between the

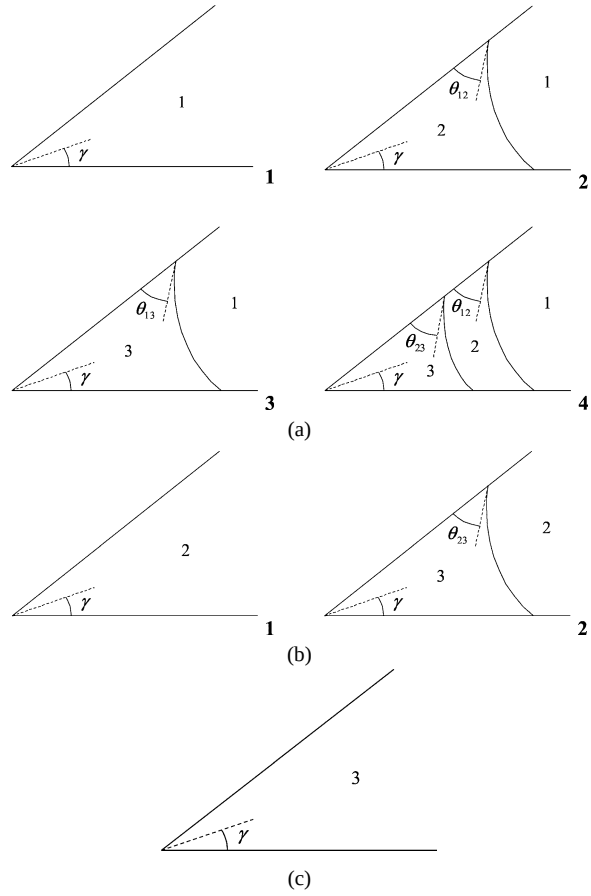

Fig. 1. Possible three-phase configurations in the corner of a pore, with (a) bulk non-wetting phase 1, (b) bulk intermediate-wetting phase 2, and (c) bulk wetting phase 3 only.

interfaces separating phases i and j, and the pore wall. Taking $\cos\theta_{ij} \geqslant 0$, i.e., $\theta_{ij} \leqslant \pi/2$, phase j is indeed wetting relative to phase i. Furthermore, we assume that the entire pore is uniformly wetted, i.e., that the oil–water contact angle is the same for the solid surface surrounding the entire pore and that also the remaining contact angles are constant throughout a pore.

According to the wetting order the center or bulk of the pore is occupied by the most non-wetting phase, i.e., phase 1 if present, otherwise phase 2 if present, while phase 3 can only occupy the center if both phases 1 and 2 are absent. On the other hand, each individual corner may be occupied according to the seven configurations sketched in Fig. 1, where the most wetting phase that is present occupies the tip of the corner. In a corner, the interfaces separating the various phases are denoted as arc menisci (AM). Assuming for the moment that a particular AM separates only one corner from the center of the pore, i.e., AMs from different corners do not interfere, the occupancy of an entire pore cross-section is determined by the bulk phase occupancy and the occupancies of the individual corners. In Section 2.2 we comment on the case when the AMs do interfere.

The actual existence of corner occupancies as sketched in Fig. 1 requires that the sketched AMs geometrically fit in the

corners. Therefore, a first simple condition for the presence of an interface between phases i and j is that

$$\theta_{ij} \leqslant \frac{\pi}{2} - \gamma. \tag{1}$$

Consequently, for a given bulk phase the configurations in Fig. 1 are mutually exclusive, except configurations 3 and 4 of Fig. 1a. For example, with bulk phase 2 we have either $\theta_{12} > \pi/2 - \gamma$, yielding configuration 1 of Fig. 1b, or $\theta_{12} \leqslant \pi/2 - \gamma$, yielding configuration 2 of Fig. 1b. With bulk phase 1 and all three contact angles satisfying $\theta_{ij} \leqslant \pi/2 - \gamma$, an additional condition is needed for the presence of an intermediate-wetting layer as sketched in configuration 4 of Fig. 1a. Fenwick and Blunt [2] and Firincioglu et al. [16] have formulated the following necessary purely geometrical condition for the existence of such a layer,

$$\frac{r_{23}}{r_{12}} \leqslant \begin{cases} \frac{\cos(\theta_{12}+\gamma)}{\cos(\theta_{23}+\gamma)} & \text{if } \theta_{23} \leqslant \theta_{12}, \\ \frac{\cos\theta_{12}-\sin\gamma}{\cos\theta_{23}-\sin\gamma} & \text{if } \theta_{23} > \theta_{12}, \end{cases} \tag{2}$$

provided that θ_{12} and θ_{23} satisfy condition (1). In condition (2) r_{ij} denotes the radius of curvature for the AM between phases i and j (see also Fig. 3).

Notice that we assume that only convex interfaces occur, defining convex as sketched in Fig. 1, since concave AMs generally do not arise from realistic displacement processes in uniformly wetted pores [13]. Consequently, we consider only positive radii of curvatures r_{ij}, when defined as in Fig. 3. Furthermore, if an interface can exist in a particular corner, its radius of curvature is bounded from above, because for too large radii AMs from different corners coalesce.

For the piston-like displacement of one bulk phase by another, we consider all possible pairs of cross-sectional fluid configurations with different bulk phases in a single pore. Obviously, the two bulk phases must meet somewhere inside the pore and are said to be separated by a main terminal meniscus (MTM). Furthermore, corner phases surrounding the bulk phase may lead to additional menisci at the MTM. To categorize these pairs of fluid configurations we again consider each corner of the pore separately and take a slice along the pore from the center into one of the corners, as shown in Fig. 2a for a triangular pore. Then, the possible pairs of configurations are sketched in Fig. 2b. For example, configuration 4 of Fig. 2b combines corner fluid configuration 3 of Fig. 1a to the left and configuration 1 of Fig. 1b to the right of the curved interface between phases 1 and 2. Pairs of corner configurations are not permissible only if one corresponding corner fluid configuration has the wetting phase 3 in the corner, which the other cannot have on the basis of condition (1). This excludes combination of configuration 2 of Fig. 1a and configuration 2 of Fig. 1b, as well as combination of configuration 4 of Fig. 1a and configuration 1 of Fig. 1b. Obviously, if the various corners of a particular cross-section are different, the pairs of configurations may be different in each corner as illustrated in Fig. 2c for two corners in an arbitrary triangle.

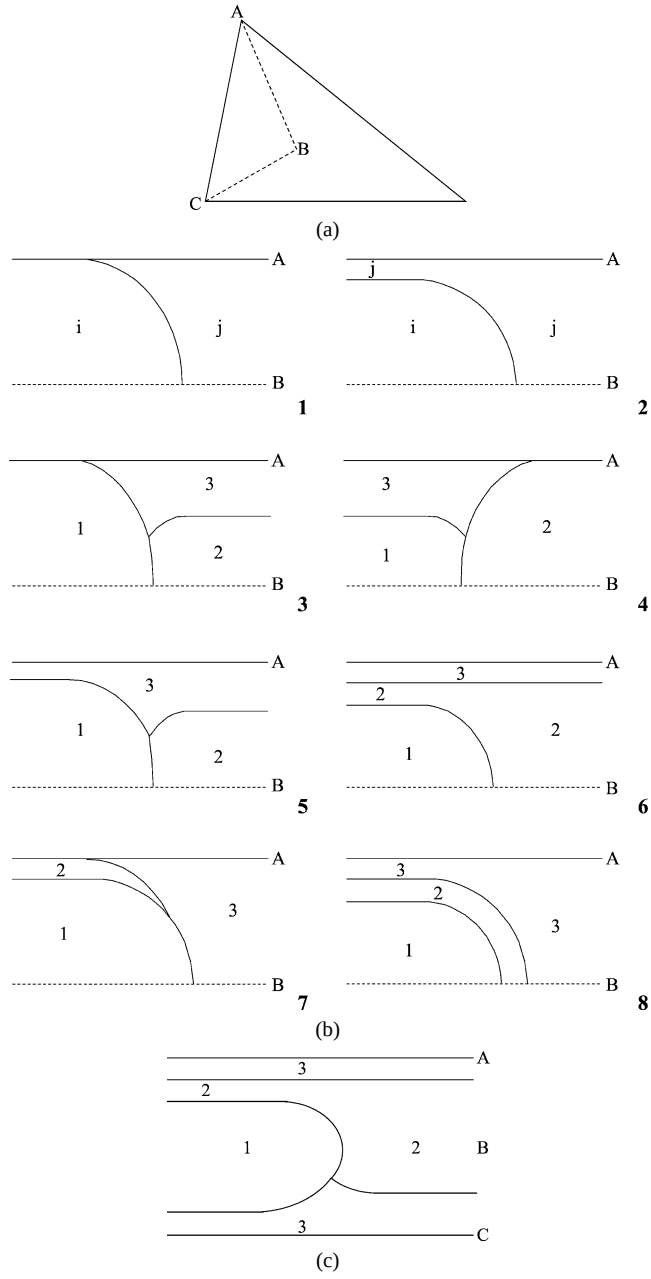

Fig. 2. (a) Cross-section of a triangular pore showing the line A–B through which a slice along the pore is taken. (b) Possible equilibrium fluid configurations in the indicated slice of the pore. (c) Possible equilibrium fluid configuration in the slice through A–B–C in the triangle of Panel a, combining configurations 5 and 6 of Panel b. In configurations 1 and 2 of Panel b, phase i is non-wetting to phase j, for the possible combinations $ij = 12, 13, 23$.

Due to the possibly complicated geometry of the pore cross-section, the precise shape of the MTM is unknown. However, this does not affect the analysis below as only the corresponding effective radius of curvature is important for the capillary entry pressures. Observe that in each of configurations 3, 4, and 5 of Fig. 2b three different menisci can be distinguished as well as a three-phase (fluid–fluid–fluid) contact line.

Since we assume capillary equilibrium between the phases, the effective radius of curvature r_{ij} of a meniscus is determined by the difference $P_{ij} = P_i - P_j$ between the pressures of phases i and j on either side of the meniscus through the Laplace equation

$$P_{ij} = \frac{\sigma_{ij}}{r_{ij}}, \tag{3}$$

with $ij = 12, 13, 23$, where σ_{ij} denotes the interfacial tension. Furthermore, by definition we have

$$P_{13} = P_{12} + P_{23}. \tag{4}$$

Obviously, an AM far away from the MTM is only curved in the cross-sectional plane of the pore as sketched in Fig. 1 and forms the arc of a circle; therefore, the corresponding r_{ij} is the radius of curvature in this plane. Since we assume that the pressure differences do not vary along the pore, the effective radii of curvature r_{ij} of the same type of fluid–fluid interfaces are identical, in particular of the MTM, despite its possibly complex geometry.

2.2. Three-phase capillary entry pressures

The described equilibrium fluid configurations with pairs of different bulk phases i and j, separated by a MTM, are taken as the configurations during a piston-like displacement. The capillary entry pressure $P_{c,ij}$ associated with this displacement is then taken as the equilibrium pressure difference between the two involved bulk phases, which is given by its effective radius of curvature r_{ij} at the MTM through Eq. (3). We assume that the shapes of the menisci do not depend on the direction of displacement, i.e., we neglect contact angle hysteresis.

To derive the effective radii associated with the capillary entry pressures, we equate the virtual work W and the change of surface free energy ΔF [28], when moving the MTMs by a small distance dx in the direction along the pore. First, we consider what the balance of W and ΔF would be if the pore cross-sections on either side of the MTM were occupied by the respective bulk phases only. Then, we adjust this balance for the presence of AMs, hence additional phases, in the corner. For the moment we assume that a particular AM separates only one corner from the bulk of the pore; i.e., AMs from different corners do not interfere. Our analysis employs the same technique as that of Mayer and Stowe [5] and Princen [6–8], but for three phases.

If the pore cross-sections on either side of the MTM are occupied by the bulk phases i and j only as in configuration 1 of Fig. 2b, the virtual work is simply given by

$$W = P_{ij} A\, dx, \tag{5}$$

where A denotes the cross-sectional area of the entire pore. The change in surface free energy is given by

$$\Delta F = (\sigma_{is} - \sigma_{js}) L_s\, dx, \tag{6}$$

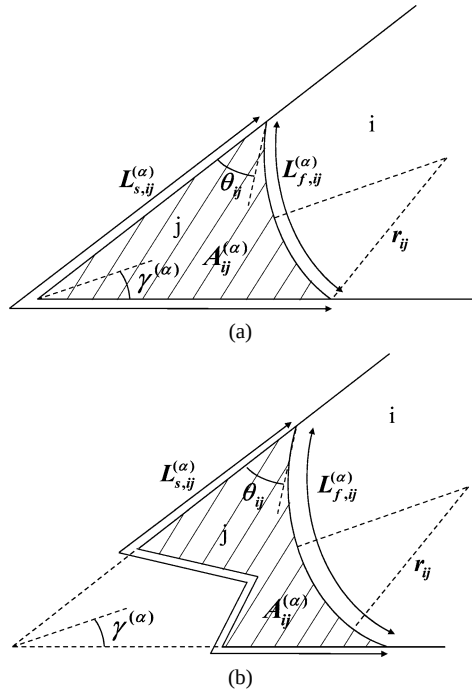

Fig. 3. (a) Cross-sectional area $A_{ij}^{(\alpha)}$ occupied by phase j in corner α in the presence of bulk phase i. The lengths of the surrounding fluid–solid and fluid–fluid contacts are indicated as $L_{s,ij}^{(\alpha)}$ and $L_{f,ij}^{(\alpha)}$, respectively. (b) Generalization if phase j occupies multiple corners.

where L_s denotes the total length of the pore walls and σ_{is} and σ_{js} denote the surface tensions for phases i and j.

If additionally one corner, indicated as α, of the pore contains AMs on one or both sides of the MTM, both the virtual work and the surface free energy change are adjusted as follows. As an example we assume that the corner has fluid configuration 5 of Fig. 2b. First, we define the cross-sectional area $A_{ij}^{(\alpha)}$ occupied by phase j in corner α in the presence of bulk phase i and the lengths of the surrounding fluid–solid and fluid–fluid contacts $L_{s,ij}^{(\alpha)}$ and $L_{f,ij}^{(\alpha)}$ as indicated in Fig. 3a. Then, the virtual work expression (5) changes into

$$W = \big(P_{12}A - P_{12}A_{23}^{(\alpha)} + P_{13}\big(A_{23}^{(\alpha)} - A_{13}^{(\alpha)}\big)\big)\, dx, \tag{7}$$

as phase 1 does not displace phase 2 in the cross-sectional area $A_{23}^{(\alpha)}$, but phase 1 does displace phase 3 in the area $A_{23}^{(\alpha)} - A_{13}^{(\alpha)}$. Furthermore, the expression for the surface free energy change (6) is adjusted to

$$\Delta F = \big((\sigma_{1s} - \sigma_{2s})L_s - \sigma_{1s}L_{s,13}^{(\alpha)} + \sigma_{2s}L_{s,23}^{(\alpha)} - \sigma_{3s}\big(L_{s,23}^{(\alpha)} - L_{s,13}^{(\alpha)}\big) + \sigma_{13}L_{f,13}^{(\alpha)} - \sigma_{23}L_{f,23}^{(\alpha)}\big)\, dx. \tag{8}$$

Equation (8) follows by considering that the fluid–solid contacts for phases 1 and 2 do not change along $L_{s,13}^{(\alpha)}$ and $L_{s,23}^{(\alpha)}$, respectively, but the contact of phase 3 does decrease along $L_{s,23}^{(\alpha)} - L_{s,13}^{(\alpha)}$. Furthermore, since on one side of the MTM an AM between phases 1 and 3 is present, which extends along the pore, and on the opposite side an AM between phases 2

and 3 is present, which shrinks, the energy changes with the respective fluid–fluid contacts of length $L_{f,13}^{(\alpha)}$ and $L_{f,23}^{(\alpha)}$.

Using definition (4), expression (7) reduces to

$$W = \left(P_{12}A - P_{13}A_{13}^{(\alpha)} + P_{23}A_{23}^{(\alpha)}\right) dx. \tag{9}$$

Furthermore, we employ Young's equation

$$\sigma_{ij}\cos\theta_{ij} = \sigma_{is} - \sigma_{js} \tag{10}$$

to reduce expression (8) to

$$\Delta F = \left(\sigma_{12}\cos\theta_{12}L_s + \sigma_{13}\left(L_{f,13}^{(\alpha)} - \cos\theta_{13}L_{s,13}^{(\alpha)}\right) - \sigma_{23}\left(L_{f,23}^{(\alpha)} - \cos\theta_{23}L_{s,23}^{(\alpha)}\right)\right) dx. \tag{11}$$

Notice, that combination of Young's equation (10) for the three fluid pairs results in the equation of Bartell and Osterhof [29]

$$\sigma_{13}\cos\theta_{13} - \sigma_{12}\cos\theta_{12} - \sigma_{23}\cos\theta_{23} = 0, \tag{12}$$

which relates the three fluid–fluid contact angles and the three interfacial tensions.

Hence, if the pore contains AMs in one corner α only, with configuration 5 of Fig. 2b, the energy balance $W = \Delta F$ for a displacement of the MTMs by a small distance dx in the direction along the pore would be

$$\left(P_{12}A - P_{13}A_{13}^{(\alpha)} + P_{23}A_{23}^{(\alpha)}\right) dx = \left(\sigma_{12}\cos\theta_{12}L_s + \sigma_{13}\left(L_{f,13}^{(\alpha)} - \cos\theta_{13}L_{s,13}^{(\alpha)}\right) - \sigma_{23}\left(L_{f,23}^{(\alpha)} - \cos\theta_{23}L_{s,23}^{(\alpha)}\right)\right) dx. \tag{13}$$

Using Eq. (3) for the various pressure differences, we may write Eq. (13) as

$$\sigma_{12}g(r_{12,}\theta_{12}) - \sigma_{13}g^{(\alpha)}(r_{13,}\theta_{13}) + \sigma_{23}g^{(\alpha)}(r_{23,}\theta_{23}) = 0, \tag{14}$$

where g and $g^{(\alpha)}$ are purely geometrical functions, defined as

$$g(r,\theta) = \frac{A}{r} - \cos\theta\, L_s, \tag{15a}$$

$$g^{(\alpha)}(r,\theta) = \frac{A^{(\alpha)}(r,\theta)}{r} + L_f^{(\alpha)}(r,\theta) - \cos\theta\, L_s^{(\alpha)}(r,\theta), \tag{15b}$$

with $A^{(\alpha)}(r_{ij},\theta_{ij}) = A_{ij}^{(\alpha)}$, $L_s^{(\alpha)}(r_{ij},\theta_{ij}) = L_{s,ij}^{(\alpha)}$, and $L_f^{(\alpha)}(r_{ij},\theta_{ij}) = L_{f,ij}^{(\alpha)}$. Obviously, $g^{(\alpha)}$ additionally depends on the half angle $\gamma^{(\alpha)}$ of the corresponding corner. A basic trigonometric exercise on the corner geometry shown in Fig. 3a gives

$$A^{(\alpha)} = r^2\left(\theta + \gamma^{(\alpha)} - \frac{\pi}{2} + \cos\theta\left(\frac{\cos\theta}{\tan\gamma^{(\alpha)}} - \sin\theta\right)\right), \tag{16a}$$

$$L_s^{(\alpha)} = 2r\left(\frac{\cos\theta}{\tan\gamma^{(\alpha)}} - \sin\theta\right), \tag{16b}$$

$$L_f^{(\alpha)} = 2r\left(\frac{\pi}{2} - \theta - \gamma^{(\alpha)}\right). \tag{16c}$$

Notice, that if an interface is absent in corner α, $A^{(\alpha)} = L_s^{(\alpha)} = L_f^{(\alpha)} = 0$, hence $g^{(\alpha)} = 0$.

Furthermore, with expressions (16), Eq. (15b) reduces to

$$g^{(\alpha)}(r,\theta) = -\frac{A^{(\alpha)}(r,\theta)}{r}. \tag{17}$$

Considering Eq. (14), we find that the first term reflects the energy balance for the bulk phase displacement if no AMs are present. The second term reflects the energy balance related to the AM surrounding bulk phase 1 and the third term reflects the energy balance related to the AM surrounding bulk phase 2. Since we assume that the AMs from different corners do not interfere, Eq. (14) can now easily be generalized for a piston-like displacement of phases i and j in a pore with n corners

$$\sigma_{ij}g(r_{ij},\theta_{ij}) - \sum_{\alpha=1}^{n}\Big(\left\{\sigma_{12}g^{(\alpha)}(r_{12},\theta_{12}) + \sigma_{13}g^{(\alpha)}(r_{13},\theta_{13}) + \sigma_{23}g^{(\alpha)}(r_{23},\theta_{23})\right\}_{\text{side } i} + \left\{\sigma_{12}g^{(\alpha)}(r_{12},\theta_{12}) + \sigma_{13}g^{(\alpha)}(r_{13},\theta_{13}) + \sigma_{23}g^{(\alpha)}(r_{23},\theta_{23})\right\}_{\text{side } j}\Big) = 0, \tag{18}$$

where sides i and j indicate the sides of the MTM where bulk phases i and j, respectively, are present.

For a given geometry and a set of σ_{ij} and θ_{ij}, Eq. (18) yields a relation between the three radii of curvature r_{ij}, $ij = 12, 13, 23$. Combination of Eqs. (3) and (4) provides an additional relation between the three radii,

$$\frac{\sigma_{13}}{r_{13}} = \frac{\sigma_{12}}{r_{12}} + \frac{\sigma_{23}}{r_{23}}, \tag{19}$$

which reduces Eq. (18) to a functional relation between at most two of the radii of curvature.

Since the pressure differences P_{ij} between the phases can directly be expressed in terms of the corresponding radii of curvature through Eq. (3), we find eventually a relation between the pressure difference between the bulk phases and one of the remaining pressure differences. The pressure difference between the bulk phases is then taken as the capillary entry pressure $P_{c,ij}$ for piston-like displacement of phases i and j, which may vary with one of the remaining pressure differences. The latter reflects the pressure in the third remaining phase, relative to the bulk phase pressures, more specifically, the pressure in the corner wetting phase 3 for bulk phase displacement of phases 1 and 2 or the pressure in the layer of intermediate-wetting phase 2 for bulk phase displacement of phases 1 and 3. In other words, given the pressure in the remaining third phase, Eqs. (18) and (19) provide the means to calculate the corresponding capillary entry pressure of the bulk phases.

Obviously, obtaining a functional relation between two of the radii of curvatures is subject to a number of physical and mathematical restrictions. The mathematical restrictions deal mainly with the issue of existence and uniqueness of solutions of Eqs. (18) and (19). We do not derive a general

theory, but address this for specific cross-sectional geometries in Section 3. With respect to uniqueness, in many cases Eq. (18) depends only on two of the radii and then contains quadratic expressions for each of these radii. This means that at most two solutions are found of which one can often be excluded by the physical restrictions on the r_{ij} that they must be positive and bounded from above, as described in Section 2.1. We define $r_{ij}^{\max}$ as the maximum allowed radius, i.e., for which all AMs of a given type coalesce. At this radius the surrounding corner phase snaps off the bulk phase on one side of the MTM and the anticipated piston-like displacement is no longer possible. In other words, the pressure in the surrounding phase relative to that in the bulk phase becomes too high to sustain a configuration with that bulk phase in the center of the pore. For most regular geometries $r_{ij}^{\max}$ can easily be calculated, considering that at this radius the bulk phase is no longer in contact with the pore wall, i.e., the total length of fluid–solid contact vanishes:

$$L_s - \sum_{\alpha} L_{s,ij}^{(\alpha)} = 0 \tag{20}$$

(see Fig. 3). Notice that $r_{ij}^{\max}$ is infinite if according to condition (1) no AMs can exist in any of the corners. The same restriction applies for r_{23} when a layer of phase 2 is present.

Similarly, the pressure in an intermediate-wetting layer can be too high relative to the pressure of either the surrounding wetting phase or the enclosed bulk phase. This is particularly important for displacements in configurations such as 7 and 8 of Fig. 2b. If the pressure in phase 2 becomes too high, phase 2 entirely separates phases 1 and 3 and piston-like displacements can occur in two steps only, i.e., phase 1 displacing phase 2 and phase 2 displacing phase 3 (compare micromodel experiments of Keller et al. [30]).

A layer of intermediate-wetting phase 2 may form under the conditions formulated in Section 2.1. When the configurations with and without a layer can both occur, it is likely that the configuration with the lowest capillary entry pressure, hence smallest equilibrium pressure difference, occurs, since the latter is directly proportional to the free energy of the system, as shown in the above derivations.

Finally, Eq. (18) can in principle also be applied in cross-sections where AMs from different corners may interfere. In this case, the index α refers to each distinguishable AM, which separates bulk phase i from phase j residing in a combination of corners, as shown in Fig. 3b. Then, the effective half angle $\gamma^{(\alpha)}$ is found as the half angle between the slopes of the pore wall at the two positions where the AM touches the pore wall. The area and lengths of fluid–fluid and fluid–solid contacts are taken as indicated in Fig. 3b. Obviously, determining which corners or combinations of corners are occupied for a given radius of curvature is in general a nontrivial exercise. Furthermore, Eq. (18) applies in principle to any cross-sectional shape as long as the effective half angle can be determined.

3. Results for specific geometries

3.1. Equilateral triangle

First, we apply the above theory to a pore, with equilateral triangular cross-section. This shape of pore has often been taken as a model pore and two-phase capillary entry conditions were derived by Ransohoff et al. [10] and Ma et al. [13]. By definition, all corners in this pore are equal, which greatly simplifies the analysis. For an equilateral triangle with side d, i.e., $\gamma = \pi/6$, we have $A = (\sqrt{3}/4)d^2$, $L_s = 3d$, and the geometrical functions for the corners are given by Eqs. (16). Using Eq. (20) we find

$$r^{\max} = \frac{r^{\text{in}}}{\cos\theta - (\sqrt{3}/3)\sin\theta}, \tag{21}$$

where $r^{\text{in}} = (\sqrt{3}/6)d$ is the radius of the inscribed circle of the triangle.

For piston-like displacement of phases i and j in the absence of a third phase, as in configurations 1 and 2 of Fig. 2b, Eq. (18) reduces to

$$\sigma_{ij}\left(g(r_{ij},\theta_{ij}) - \sum_{\alpha=1}^{3} g^{(\alpha)}(r_{ij},\theta_{ij})\right) = 0, \tag{22}$$

where $g^{(\alpha)} = 0$ for configuration 1 of Fig. 2b. Obviously, Eq. (22) depends on only one type of radius r_{ij} and its solution does not depend on σ_{ij}. Interestingly, if a layer of phase 2 is present in all corners, as in configuration 6 of Fig. 2b, we also find Eq. (22), for $ij = 12$, since the contributions $g^{(\alpha)}$ related to the AMs between phases 2 and 3 on either side of the MTM cancel. Using expressions (16), we readily find the simple solution of Eq. (22), denoted as r_{ij}^{s}, as [10,13]

$$r_{ij}^{s} = \begin{cases} \dfrac{r^{\text{in}}}{\cos\theta_{ij} + \sqrt{(1/\sqrt{3})(\pi/3 - \theta_{ij} + \sin\theta_{ij}\cos\theta_{ij})}} & \text{if } \theta_{ij} < \dfrac{\pi}{3}, \\ \dfrac{r^{\text{in}}}{2\cos\theta_{ij}} & \text{if } \theta_{ij} \geqslant \dfrac{\pi}{3}. \end{cases} \tag{23}$$

The presented solution for $\theta_{ij} < \pi/3$ is the only one of the possible two that satisfies $0 < r_{ij} < r_{ij}^{\max}$. Obviously, this solution does not depend on any of the other radii, i.e., the corresponding $P_{c,ij}$ is independent of the pressure of the remaining third phase. The latter is the common assumption for displacements in three-phase flow [18–25]; therefore, Eq. (22) is the basis of all capillary entry pressures employed in the three-phase flow pore-scale models described in the mentioned references. However, in general we find more complicated expressions if we allow the third phase to be present in the pore.

The radii of curvature associated with piston-like displacement of phases 1 and 2 in the presence of phase 3, as in configurations 3, 4, and 5 of Fig. 2b, follow from Eq. (18) as

$$\sigma_{12}g(r_{12},\theta_{12}) - \sum_{\alpha=1}^{3}\big(\sigma_{13}g^{(\alpha)}(r_{13},\theta_{13}) - \sigma_{23}g^{(\alpha)}(r_{23},\theta_{23})\big) = 0, \tag{24}$$

where the contributions $g^{(\alpha)}$ corresponding to r_{13} and r_{23} vanish for configurations 3 and 4 of Fig. 2b, respectively. Obviously, this equation depends on more than one radius of curvature; therefore, the capillary entry pressure $P_{c,12}$ depends on the pressure of phase 3. Since no AM between phases 1 and 2 occurs, Eq. (24) can be rewritten using Eqs. (14), (15a), and (19) as

$$\sigma_{13}\left(g(r_{13},\theta_{13})-\sum_{\alpha=1}^{3}g^{(\alpha)}(r_{13},\theta_{13})\right) = \sigma_{23}\left(g(r_{23},\theta_{23})-\sum_{\alpha=1}^{3}g^{(\alpha)}(r_{23},\theta_{23})\right). \quad (25)$$

Equation (25) consists of two terms of which each depends on one radius of curvature only. Moreover, if one radius, representing the pressure in phase 3 relative to one of the bulk phases, is given, the remaining radius in Eq. (25) can be calculated. Notice that each of the terms in Eq. (25) has the same form as that in Eq. (22). With expressions (16), Eq. (25) can be formulated as a quadratic equation for one of the radii, which has an explicit but lengthy solution. Eq. (19) now yields the desired radius r_{12}.

Similar to Eq. (25), we find for the displacement of phases 1 and 3 according to configurations 7 and 8 of Fig. 2b

$$\sigma_{12}\left(g(r_{12},\theta_{12})-\sum_{\alpha=1}^{3}g^{(\alpha)}(r_{12},\theta_{12})\right) = -\sigma_{23}\left(g(r_{23},\theta_{23})-\sum_{\alpha=1}^{3}g^{(\alpha)}(r_{23},\theta_{23})\right), \quad (26)$$

where the contribution $g^{(\alpha)}$ corresponding to r_{23} vanishes for configuration 7 of Fig. 2b.

For a series of fluid–fluid parameters, which are given in Table 1, we have calculated the relations between the various radii of curvatures. The radii are normalized as $\rho = r/r^{\text{in}}$. In Table 1 the ratios of the interfacial tensions σ_{12}/σ_{23} and σ_{13}/σ_{23} are specified, as well as the contact angles θ_{ij}. Obviously, given two of the contact angles, the remaining third must satisfy Eq. (14). The actual choice of values of contact angles further obeys the linear relations [31,32]

$$\cos\theta_{\text{go}} = \frac{1}{2\sigma_{\text{go}}}\{C_{s,o}\cos\theta_{\text{ow}} + C_{s,o} + 2\sigma_{\text{go}}\}, \quad (27a)$$

$$\cos\theta_{\text{gw}} = \frac{1}{2\sigma_{\text{gw}}}\big\{(C_{s,o} + 2\sigma_{\text{ow}})\cos\theta_{\text{ow}} + C_{s,o} + 2\sigma_{\text{go}}\big\}, \quad (27b)$$

where $C_{s,o}$ is the oil spreading coefficient and the contact angles are measured through the phase indicated by the second subscript. These relations reflect the assumption that not two but only one contact angle is known, i.e., $\cos\theta_{\text{ow}}$ for oil–water, which reflects the underlying wettability of the pore. Obeying relations (27), means that we can envisage a realistic situation for each of the cases in Table 1, i.e., for cases 1 to 4 and 7 we take the wetting order $1 = g$, $2 = o$, $3 = w$, reflecting the situation in water-wet pores. For cases 5 and 6 we take the wetting order $1 = g$, $2 = w$, $3 = o$, reflecting the situation in oil-wet pores with water wetting to gas. These orders are also in agreement with the most likely scenario in which the gas–water interfacial tension is larger than the remaining two.

Table 1
Fluid–fluid parameters (interfacial tensions, contact angles, and spreading coefficient for phase 2, $C_{s,2}$) for calculation of the relations between the various radii of curvature at the entry conditions for piston-like displacement between phases 1 and 2 (1 displ. 2) or phases 1 and 3 (1 displ. 3)

Case	$\frac{\sigma_{12}}{\sigma_{23}}$	$\frac{\sigma_{13}}{\sigma_{23}}$	θ_{12}	θ_{13}	θ_{23}	$\frac{C_{s,2}}{\sigma_{23}}$	Fig. (1 displ. 2)	Fig. (1 displ. 3)
1	0.6	1.6	0	0	0	0	2b5/2b6	2b2/2b8
2	0.8	1.6	0.663	0.593	0.8	−0.2	2b5/2b6	
3	0.6	1.6	0	0.925	1.2	0	2b2/2b4	2b2/2b7
4	0.8	1.2	1.32	0	0	−0.6	2b5	
5	1.6	0.8	1.16	0.487	1.5	−1.8	2b4	
6	1.6	0.8	1.44	0.341	1.0	−1.8	2b5	
7	0.8	1.6	0.699	0.373	0.5	−0.2	N/A	

Note. Cases 1 to 6 correspond to a pore of triangular cross-section and case 7 to a pore of rhomboidal cross-section. Furthermore, the figures are indicated which reflect the corresponding corner fluid configurations.

Furthermore, we have chosen the interfacial tensions such that the spreading coefficient of the intermediate-wetting phase 2, $C_{s,2} = \sigma_{13} - \sigma_{12} - \sigma_{23}$, is less than or equal to zero, reflecting conditions of thermodynamic equilibrium [28]. In fact, the remaining spreading coefficients, $C_{s,1} = \sigma_{23} - \sigma_{12} - \sigma_{13}$ and $C_{s,3} = \sigma_{12} - \sigma_{13} - \sigma_{23}$, satisfy the same condition. If $C_{s,2} = 0$, phase 2 separates phases 1 and 3 at least by a molecularly thin spreading film.

In Fig. 4 we present the normalized radii of curvature for piston-like displacement of phases 1 and 2. For example, in Fig. 4a, where the parameters of case 1 apply, we have calculated ρ_{13} as a function of ρ_{23} using Eq. (25). Then ρ_{12} follows from Eq. (19). This solution is based on corner fluid configuration 5 of Fig. 2b. Because this solution is not constant, the corresponding capillary entry pressure $P_{c,12}$ varies, not monotonically, with the pressure in the corner phase 3, reflected by the pressure difference P_{23} corresponding to ρ_{23}. On the other hand, ρ_{12}^{s} is the simple solution given by the first expression in Eq. (23), assuming that a layer of phase 2 separates phases 1 and 3 as in configuration 6 of Fig. 2b. The corresponding capillary entry pressure does not depend on the pressure of phase 3. The validity of both solutions is restricted to values of ρ_{23} less than $\rho_{23}^{\max}$, for which phase 3 snaps off phase 2. Similarly, the corresponding ρ_{13} must be less than $\rho_{13}^{\max}$ to avoid snap-off of phase 1 by phase 3. The straight dashed line delineates part of the (ρ_{23}, ρ_{12}) space where inequality (2) is satisfied. Only below this line a layer of phase 2 may be present; i.e., ρ_{12}^{s} may be valid.

The parameters of case 1 reflect the situation for a spreading oil in a strongly water-wet pore. Then, the curves for ρ_{12} and ρ_{12}^{s} in Fig. 4a touch exactly at the point where the line corresponding to inequality (2) crosses these curves.

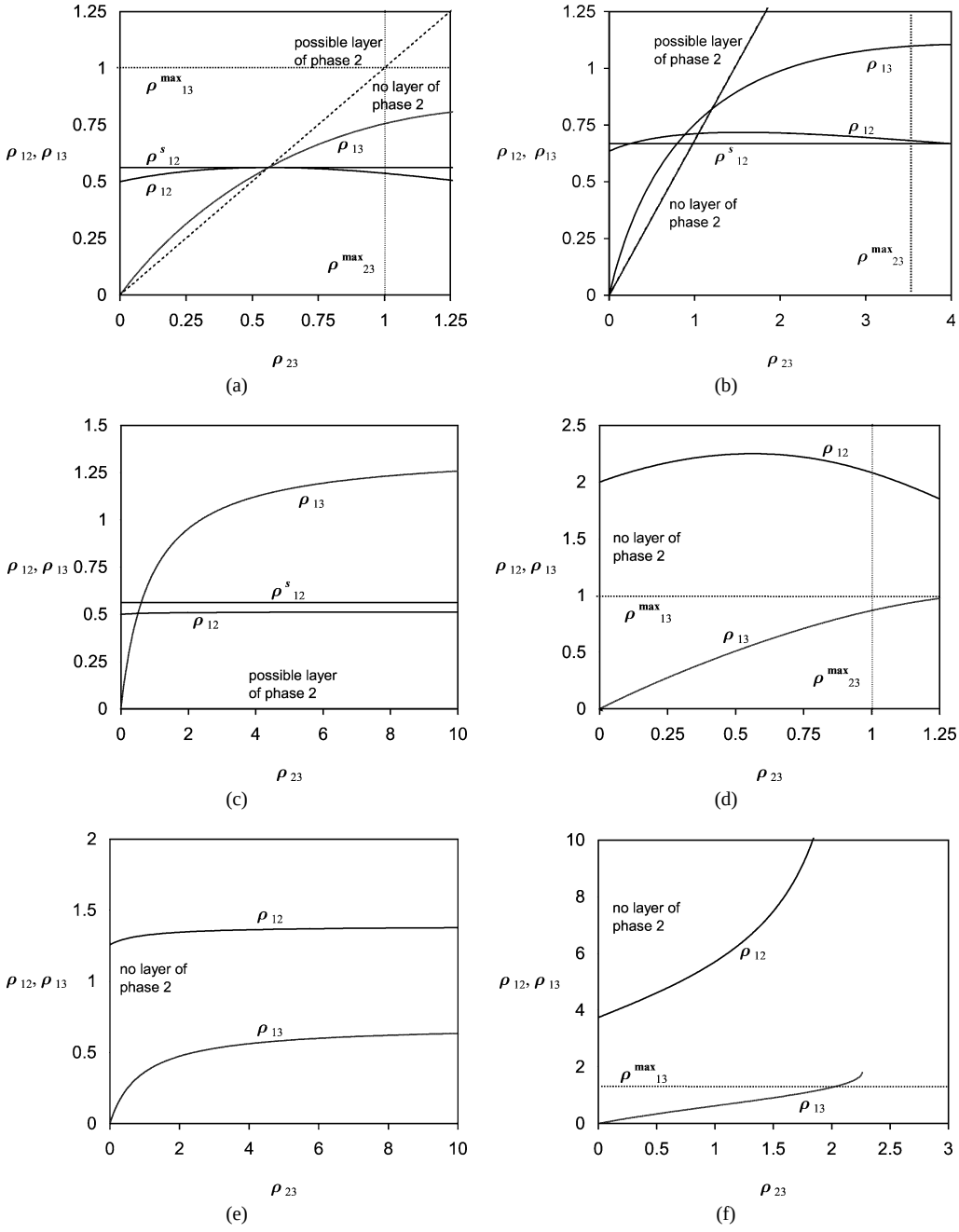

Fig. 4. Normalized radii of curvature corresponding to the capillary entry pressure for piston-like displacement of phases 1 and 2, ρ_{12} and ρ_{12}^s, in a pore of triangular cross-section, as functions of the normalized radius ρ_{23}, which reflects the pressure in the corner wetting phase 3. ρ_{12}^s denotes the (constant) radius when a layer of phase 2 is assumed to be present, whereas ρ_{12} is the solution in the absence of a layer. ρ_{13} is the intermediate result in calculating ρ_{12}. The maximum radii $\rho_{ij}^{\max}$ correspond to snap-off events and denote the maximum possible radii for which piston-like displacement can occur. Furthermore, a straight dashed line may be present, calculated from condition (2), to indicate values of ρ_{12} for which a layer of phase 2 may or may not be present. Panels a–f correspond to cases 1–6 in Table 1, respectively.

Hence, for ρ_{23} larger than the ρ_{23} corresponding to this point, ρ_{12} is the only possible solution. For smaller ρ_{23}, a layer may be present and the capillary entry condition is derived from ρ_{12}^s. Notice that in this case ρ_{12} is always smaller than ρ_{12}^s; hence, the absolute value of $P_{c,12}$ is larger for the case without than with a film, making ρ_{12}^s more likely. Anyway, the quantitative difference between the two solutions is small, but this may be different for geometries other than equilateral triangular. Additionally, if the contact angles do not obey the linear relations (27), the difference can become larger.

Case 2 reflects the situation for a nonspreading oil in a weakly water-wet pore. Figure 4b indicates that, contrary to case 1, most of the ρ_{12} lies above ρ_{12}^s. Based on the above argument for the absolute value of $P_{c,12}$, ρ_{12}^s is only a likely option for ρ_{23} between 0 and the first crossover of ρ_{12}

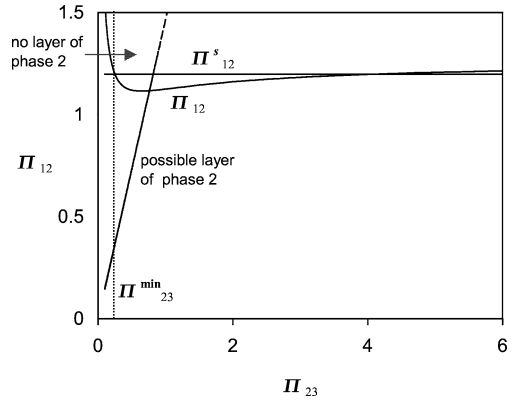

Fig. 5. Normalized capillary entry pressure for piston-like displacement of phases 1 and 2, Π_{12} and Π^s_{12}, in a pore of triangular cross-section for the parameters of case 2 in Table 1, as functions of the normalized pressure difference Π_{23}, which reflects the pressure in the corner wetting phase 3. Π^s_{12} denotes the (constant) capillary entry pressure when a layer of phase 2 is assumed to be present, whereas Π_{12} is the solution in the absence of the latter. Based on condition (2) the space is divided into sections where a phase 2 layer can or cannot possibly be present.

and ρ^s_{12}. Notice that the larger value of $\rho^{\max}_{23}$ for the increased contact angle has extended the range of allowed ρ_{23}, which is expected as for more weakly water-wet pores snap-off is less likely [33].

To illustrate the behavior of the corresponding capillary entry pressures, Fig. 5 shows the normalized entry pressures, Π_{12} and Π^s_{12}, as a function of the normalized pressure difference between phases 2 and 3, Π_{23}, where $\Pi = Pr_{\text{in}}/\sigma_{23}$. Obviously, the maximum radius $\rho^{\max}_{23}$ transforms into a minimum allowed pressure difference $\Pi^{\min}_{23}$. Because of the inverse proportionality between radius and pressure, the small range of radii for which the solution with a layer is possible, as shown in Fig. 4b, transforms into a large range of pressure differences in Fig. 5. However, as we may expect that the various pressure differences are of the same order of magnitude, the solution without a layer is the more likely option for most realistic pressure differences. Notice that the quantitative difference between Π_{12} and Π^s_{12} is not very large.

For case 3, which reflects a very weakly water-wet pore with a spreading oil, the oil–water contact angle θ_{23} does not satisfy condition 1. Hence, this situation corresponds to fluid configuration 2, with $i = 1$ and $j = 2$, or 4 of Fig. 2b. Strictly speaking, configuration 2 of Fig. 2b does not involve a layer of phase 2 that separates phases 1 and 3, but we still refer to this configuration as having a layer, because the corresponding solution for the radius of curvature is given by (the first expression in) Eq. (23). Furthermore, snap-off of phase 2 by phase 3 is no longer possible; hence, for the solutions shown in Fig. 4c all (positive) values of ρ_{23} are allowed. Inequality (2) allows a solution with a layer for all ρ_{23}. Notice that also the varying solution is almost constant. For case 4, which reflects a strongly water-wet pore with strongly negative oil spreading coefficient, the gas–oil contact angle θ_{12} does not satisfy condition 1. Then, an AM between phases 1 and 2 cannot be present and only

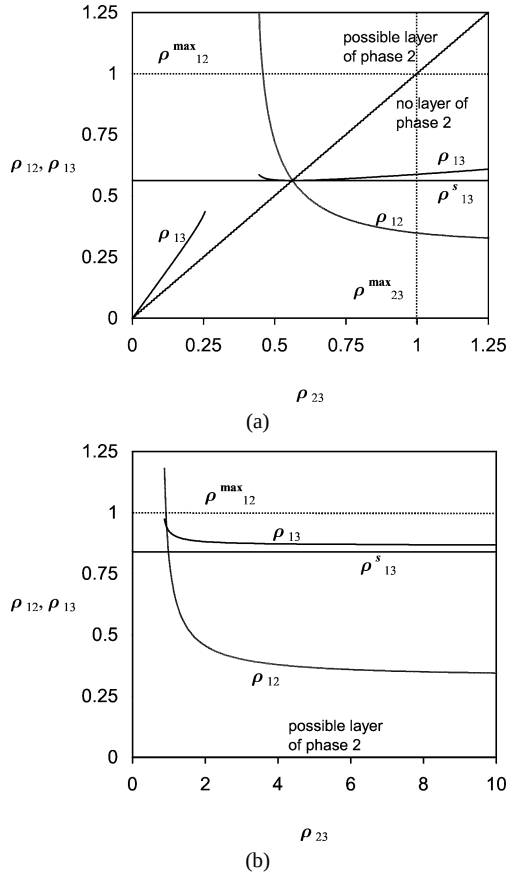

Fig. 6. Normalized radii of curvature corresponding to the capillary entry pressure for piston-like displacement of phases 1 and 3, ρ_{13} and ρ^s_{13}, in a pore of triangular cross-section, as functions of the normalized radius ρ_{23}, which reflects the pressure in the corner wetting phase 3. Panels a and b correspond to cases 1 and 3 in Table 1, respectively.

configuration 5 of Fig. 2b, without a layer, is possible. The resulting solution ρ_{12}, shown in Fig. 4d, shows significant variation with ρ_{23}. On the other hand, if both θ_{13} and θ_{23} do not satisfy condition (1), only a constant solution is possible.

Cases 5 and 6 reflect conditions for a weakly oil-wet pore in which water is wetting to gas and the water spreading coefficient is strongly negative. Not surprisingly, condition (2) indicates that no layer of phase 2 can be present. For case 5 both θ_{12} and θ_{23}, the gas–water and water–oil contact angles, respectively, do not satisfy condition (1). Hence, only configuration 4 of Fig. 2b is possible for which, the corresponding solution ρ_{12} is shown in Fig. 4e. This solution does not show much variation with ρ_{23}. Case 6, where only θ_{12} does not satisfy condition (1), corresponds to configuration 5 of Fig. 2b. In this situation the variation in the associated solution ρ_{12} is huge, as for $\rho_{23} = 2.25$ both ρ_{12} and ρ_{13} go to infinity. However, the validity is restricted by the snap-off value $\rho^{\max}_{13}$ for ρ_{13}, such that ρ_{23} is not allowed to be larger than 2.06 with $\rho_{12} = 14.3$. This case is exemplary for a strong dependence of the capillary entry pressure on the corner phase pressure.

In Fig. 6 we present the radii of curvature associated with piston-like displacement of phases 1 and 3 for two different sets of parameters that may lead to entry conditions which

depend on the pressure of phase 2. To find any effect of the latter, a layer of phase 2 needs to be present; hence, if $\theta_{12} > \pi/3$ we know a priori that such a varying solution for ρ_{13} cannot be found. In Fig. 6a the radii of curvature for the parameters of case 1 are shown, corresponding to spreading conditions in a strongly water-wet pore. A possible varying solution ρ_{13} corresponds to fluid configuration 8 of Fig. 2b, while a constant solution ρ_{13}^s corresponds to configuration 2 of Fig. 2b, with $i = 1$ and $j = 3$.

For $\rho_{23} = 0.441$, ρ_{12} and ρ_{13} become infinite and below this value only negative solutions of ρ_{12} are found. Then, the restrictions $\rho_{12}^{\max}$ and $\rho_{23}^{\max}$ allow the varying solution ρ_{13} to $0.458 < \rho_{23} < 1$ only. Condition (2) for the existence of a layer of phase 2, indicated in Fig. 6a, restricts this range of allowed values of ρ_{23} even further to $0.458 < \rho_{23} < \rho_{23}^s = 0.563$, where $\rho_{23} = \rho_{23}^s$ is the solution of Eq. (22) for $ij = 23$, while at this point also $\rho_{12} = \rho_{12}^s$, see Eq. (26). Finally, we find that for $\rho_{23} \leqslant \rho_{23}^s$, hence $\rho_{12} \geqslant \rho_{12}^s$, the pressure in phase 2 becomes too high to allow the piston-like displacement of phases 1 and 3. Instead, for these values of ρ_{23} two separate piston-like displacements will take place as discussed at the end of Section 2.2. Consequently, for the present case where phase 2 is spreading and the pore is strongly water-wet, piston-like displacement with a layer of phase 2 is impossible.

In Fig. 6b, we show the solutions for the radii of curvature for the parameters of case 3, which also reflects a situation involving a spreading oil, but where the pore is weakly water-wet, such that the oil–water contact angle θ_{23} does not satisfy condition (1). As condition (2) is satisfied for all positive ρ_{12} and ρ_{23}, a layer of phase 2 may always be present surrounding phase 1, as shown in configuration 7 of Fig. 2b. This leads to a varying solution ρ_{13} whose validity is restricted by ρ_{23}^s only; i.e., ρ_{13} is valid for $\rho_{23} > 1.38$. Since θ_{13} also satisfies condition (1), the alternative constant solution ρ_{13}^s corresponds to configuration 2 of Fig. 2b with $i = 1$ and $j = 3$. Notice that the varying and constant solutions are significantly different and that the varying solution ρ_{13} is the most likely one, but that this solution does not vary much with the pressure in phase 3.

3.2. Rhombus

Contrary to the equilateral triangular cross-section, a typical example of a cross-section in which not all corners are equal is the rhombus. This may lead to additional complications when condition (1) is satisfied only in some of the corners, although the corresponding geometrical functions are still easily analyzable. In Fig. 7a we present the geometry of the rhombus and we define the aspect ratio $a = r_w/r_d$, which is the most characteristic parameter. In Fig. 7b we show a fluid configuration with different corner occupancies, when for example θ_{12} is satisfied in corners 1 and 3, but not in corners 2 and 4.

The area and perimeter for the rhombus are $A = 2r_w r_d$ and $L_s = 4d$, whereas the geometrical functions for the

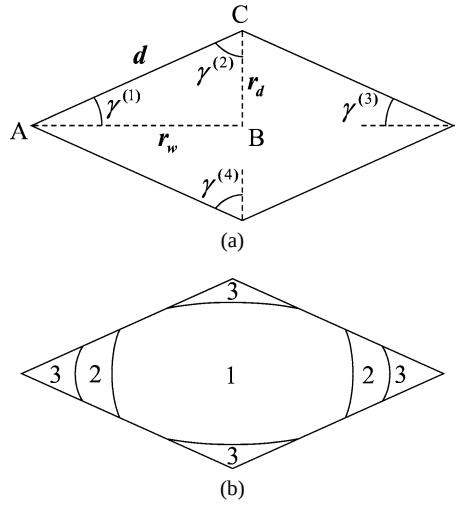

Fig. 7. (a) Geometry of rhombus with principal radii $r_d \leqslant r_w$, side $d = \sqrt{r_w^2 + r_d^2}$, and corner half angles $\gamma^{(1)} = \gamma^{(3)} \leqslant \gamma^{(2)} = \gamma^{(4)}$. (b) Cross-sectional fluid configuration with different corner occupancies.

corners are given by Eqs. (16), where

$$\tan\gamma^{(1)} = \frac{1}{\tan\gamma^{(2)}} = \frac{r_d}{r_w}.$$

Using Eq. (20), we find

$$r^{\max} = \frac{r^{\text{in}}}{\frac{1}{d^2}((r_w^2\cos\theta - r_w r_d\sin\theta) + (r_d^2\cos\theta - r_w r_d\sin\theta))}, \tag{28}$$

where the last term in the denominator vanishes if the corresponding AM is present only in corners 1 and 3 and $r^{\max}$ is infinite if the AM is absent in all corners. $r^{\text{in}} = r_d r_w/d$ denotes the radius of the inscribed circle of the rhombus.

It may be clear that the simultaneous presence in corners 1 and 3 and absence in corners 2 and 4 of one type of AM can lead to computational complications, as for example in the configuration of Fig. 7b. An example of the corresponding fluid configuration in a slice of the pore is shown in Fig. 2c, which combines corner configurations 5 and 6 of Fig. 2b. Rather than working through all possible configurations, we consider one example for which we fix the contact angles in the order $\theta_{13} < \theta_{23} < \theta_{12}$ ($1 = g$, $2 = o$, $3 = w$ in a weakly water-wet pore), see case 7 in Table 1, and vary the corner angles by increasing the aspect ratio a from 1 (square) onward.

In Fig. 8 we present the radii of curvature for piston-like displacement of phases 1 and 2 in a pore of rhomboidal cross-section for different values of the aspect ratio $a = r_w/r_d$. For a square pore, $a = 1$, all three contact angles satisfy condition (1) in all corners and the possible solutions ρ_{12} and ρ_{12}^s, shown in Fig. 8a, are comparable to those for a similar case in the triangular pore (see case 2 in Table 1 and Fig. 4b). The equations corresponding to ρ_{12} and ρ_{12}^s are of the same form as Eqs. (22) and (25), respectively. For all four corners ρ_{12}^s corresponds to configuration 6 and ρ_{12} cor-

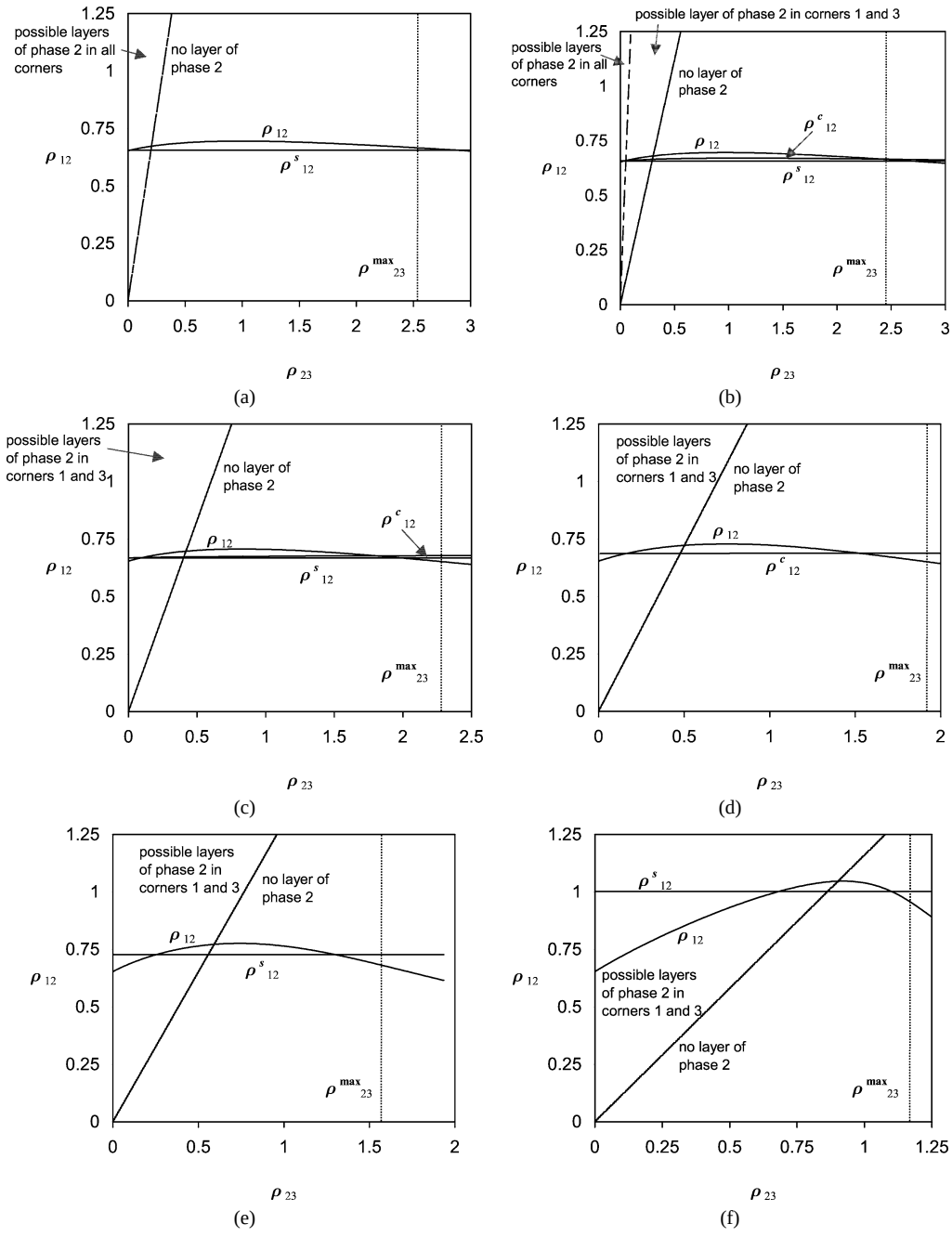

Fig. 8. Normalized radii of curvature corresponding to the capillary entry pressure for piston-like displacement of phases 1 and 2, ρ_{12}, ρ_{12}^s, and ρ_{12}^c, in a pore of rhomboidal cross-section, as functions of the normalized radius ρ_{23}, which reflects the pressure in the corner wetting phase 3. Parameters are as for case 7 in Table 1 with aspect ratios (a) $a = 1$, (b) $a = 1.15$, (c) $a = 1.5$, (d) $a = 2$, (e) $a = 3$, and (f) $a = 25$.

responds to configuration 5 of Fig. 2b. The range of values of ρ_{23} where ρ_{12} is valid is only restricted by $\rho_{23}^{\max}$. A layer of phase 2, hence ρ_{12}^s, is possible only for small values of ρ_{23}.

For $a = 1.15$, all three contact angles remain to satisfy condition (1) in all corners, but condition (2) becomes different for corners 1 and 2. The solutions ρ_{12}^s and ρ_{12} are as for $a = 1$, with layers of phase 2 in all corners and layers nowhere, respectively. A third solution, indicated as ρ_{12}^c, is possible, when only in corners 1 and 3 layers are present, for which the fluid configuration is shown in Fig. 7b. The corresponding equation is

$$\sigma_{12}g(r_{12},\theta_{12}) - \sum_{\alpha=1,3}\sigma_{12}g^{(\alpha)}(r_{12},\theta_{12}) - \sum_{\alpha=2,4}\left\{\sigma_{13}g^{(\alpha)}(r_{13},\theta_{13}) - \sigma_{23}g^{(\alpha)}(r_{23},\theta_{23})\right\} = 0. \quad (29)$$

This equation cannot easily be cast in a form with two terms for r_{13} and r_{23} separately as has been done in Eq. (25), basically because terms corresponding to all three types of AM occur. Using Eq. (19), we solve Eq. (29) for r_{12} by

the Newton–Raphson method for a given value of r_{23}. As expected, the solution ρ_{12}^c lies between ρ_{12}^s and ρ_{12} and may only be valid between the two straight lines resulting from condition (2) for the different corners, as indicated in Fig. 8b. Anyway, the deviation of ρ_{12}^c from ρ_{12}^s is small, indicating that the contributions from AMs in corners 2 and 4 are small.

For $a = 1.5$, θ_{12} ceases to satisfy condition (1) in corners 2. Hence, only solutions ρ_{12}, with no layers, and ρ_{12}^c, with layers in corners 1 and 3 only, are possible, whereas the validity of ρ_{12}^c is at least restricted by condition (2), as shown in Fig. 8c. ρ_{12}^c is again calculated from Eq. (29). Also for $a = 2$, where both θ_{12} and θ_{23} do not satisfy condition (1) in corners 2 and 4, a constant solution ρ_{12}^s does not exist. In this case a solution ρ_{12} arises, shown in Fig. 8d, with fluid configuration 5 of Fig. 2b in corners 1 and 3 and with fluid configuration 4 in corners 2 and 4. The underlying equation is similar to Eq. (25). A second varying solution ρ_{12}^c may arise when in corners 1 and 3 layers are present, thus combining configurations 4 and 6 of Fig. 2b, for which the equation is given by

$$\sigma_{12}g(r_{12},\theta_{12}) - \sum_{\alpha=1,3} \sigma_{12}g^{(\alpha)}(r_{12},\theta_{12}) - \sum_{\alpha=2,4} \sigma_{13}g^{(\alpha)}(r_{13},\theta_{13}) = 0. \tag{30}$$

As only terms relating to two different AMs arise, this equation can be cast in a simple form with separate terms for r_{12} and r_{13}, similar to Eq. (25). The validity of ρ_{12}^c is restricted by condition (2) for corners 1 and 3 as indicated. This solution is almost constant.

For $a = 3$ and $a = 25$ none of the contact angles satisfies condition (1) in corners 2 and 4. A varying solution ρ_{12}, if no layers are present, and a constant solution ρ_{12}^s, if layers are present in corners 1 and 3 only, may arise as shown in Figs. 8e and 8f, respectively. The variation of ρ_{12} with ρ_{23} clearly increases with a, but also the range of values of ρ_{23}, for which ρ_{12}^s is possible based on condition (2) becomes larger. Based on the size of the corresponding capillary entry pressures, we may expect that ρ_{12}^s is valid for ρ_{23} between 0 and the first crossover of ρ_{12} and ρ_{12}^s.

4. Summary and conclusions

We have derived a general formula for determination of the capillary entry pressures for piston-like displacement of two bulk phases in a pore with constant angular cross-section where also a third phase may be present. The method assumes that all the possible underlying phase occupancies in cross-sections on either side of the MTM are known. Using this approach, the fundamental question of whether a displacement in three-phase flow is the same as in a two-phase situation can be answered. The complexity of the corresponding equations and the quantitative effects are studied using two different geometries, the equilateral triangle and the rhombus. The main difference is that the latter geometry has unequal corners, which may carry different corner AMs. We have carried out a limited sensitivity study with respect to the effect of wettability, the spreading coefficient of the intermediate-wetting phase and the aspect ratio of the principal radii of the rhombus.

Conclusions are as follows:

(i) The capillary entry pressures for piston-like displacement of two bulk phases does depend on the pressure in the remaining third phase, if the cross-sectional fluid configurations contain this phase. Under these conditions a displacement in three-phase flow is different from a displacement in two-phase flow and the corresponding capillary entry pressure is not a combination of two-phase capillary entry pressures. The only exception arises in a displacement of the non-wetting phase 1 and the intermediate-wetting phase 2, when phase 1 is completely separated from the wetting phase 3 by layers of phase 2. If a capillary entry pressure depends on the pressure of the third phase, we refer to it as "varying," otherwise it is called "constant."

(ii) The method is subject to a number of restrictions of which the most important are (a) if the radius of curvature associated with one of the AMs, that is assumed present, becomes too large (for example, if the pressure in the corner wetting phase is too high), one of the bulk phases cannot be present in the pore and the piston-like displacement does not take place; and (b) layers of phase 2 can only be present for a limited range of radii of curvatures as indicated by condition (2). The presence or absence of such layers may give the alternative solutions, constant or varying of which the one with the smallest capillary entry pressure is the most likely.

(iii) For pores of triangular cross-section the effects of the degree of wettability (size of contact angles) and the effect of the spreading coefficient of the intermediate-wetting phase have been investigated. For a spreading oil in a water-wet pore, the varying solution for the capillary entry pressure for displacement of bulk phases 1 and 2 is less favorable than the constant solution involving layers of phase 2. For weakly water-wet pores and for oil-wet pores, the constant solution is less likely or not possible at all and the remaining varying solutions often show strong dependence on the pressure in the wetting phase 3. For displacement of bulk phases 1 and 3 the varying solution may not be allowed at all, or its dependence on the pressure in the intermediate-wetting phase 2 is weak.

(iv) In rhomboidal pores the dependence of the capillary entry pressure on the pressure in the remaining third phase increases with increasing aspect ratio. For intermediate sized aspect ratios, constant solutions do not arise, as only the smaller corners carry layers of phase 2. Because of the different sized corners additional solutions may arise, which are more complicated when all three types of AMs are present.

Acknowledgments

The authors thank the following members of the Heriot-Watt WAG Consortium for supporting this research: The UK Department of Trade and Industry, BP, Shell, PDVSA, BHP, TotalFinaElf, Norsk Hydro, and Statoil.

References

[1] R. Lenormand, C. Zarcone, in: Proceedings of the SPE Annual Technical Conference and Imbibition, Houston, 1984, SPE13264.
[2] D.H. Fenwick, M.J. Blunt, in: Proceedings of the 8th European Symposium on Improved Oil Recovery, Vienna, Austria, 1995.
[3] J.-C. Moulu, O. Vizika, F. Kalaydjian, J.-P. Duquerroix, in: Proceedings of the SPE Annual Technical Conference and Exhibition, San Antonio, 1997, SPE38891.
[4] M. Dong, F.A.L. Dullien, I. Chatzis, J. Colloid Interface Sci. 172 (1995) 278–288.
[5] R.P. Mayer, R.A. Stowe, J. Colloid Interface Sci. 20 (1965) 893–911.
[6] H.M. Princen, J. Colloid Interface Sci. 30 (1969) 69–75.
[7] H.M. Princen, J. Colloid Interface Sci. 30 (1969) 359–371.
[8] H.M. Princen, J. Colloid Interface Sci. 34 (1970) 171–184.
[9] B. Legait, J. Colloid Interface Sci. 96 (1983) 28–38.
[10] T.C. Ransohoff, P.A. Gauglitz, C.J. Radke, AIChE J. 33 (1987) 753–765.
[11] G. Mason, N.R. Morrow, J. Colloid Interface Sci. 141 (1991) 262–274.
[12] A.R. Kovscek, H. Wong, C.J. Radke, AIChE J. 39 (1993) 1072–1085.
[13] S. Ma, G. Mason, N.R. Morrow, Colloids Surf. A 117 (1996) 273–291.
[14] P.E. Øren, S. Bakke, O.J. Arntzen, SPE J. 3 (1998) 324–336.
[15] D. Zhou, M. Blunt, F.M. Orr, J. Colloid Interface Sci. 187 (1997) 11–21.
[16] T. Firincioglu, M.J. Blunt, D. Zhou, Colloids Surf. A 155 (1999) 259–276.
[17] G.G. Pereira, Phys. Rev. E 59 (1999) 4229–4242.
[18] W.E. Soll, M.A. Celia, Adv. Water Resources 16 (1993) 107–126.
[19] P.E. Øren, W.V. Pinczewski, Transport Porous Media 20 (1995) 105–133.
[20] G.G. Pereira, W.V. Pinczewski, D.Y.C. Chan, L. Paterson, P.E. Øren, Transport Porous Media 24 (1996) 167–201.
[21] D.H. Fenwick, M.J. Blunt, Adv. Water Resources 21 (1998) 121–143.
[22] V. Mani, K.K. Mohanty, SPE J. 3 (1998) 238–248.
[23] C. Laroche, O. Vizika, F. Kalaydjian, in: Proceedings of the SPE Annual Technical Conference and Exhibition, Houston, TX, 1999, SPE56674.
[24] T.W. Patzek, in: Proceedings of the SPE/DOE Improved Oil Recovery Symposium, Tulsa, OK, 2000, SPE59312.
[25] T.R. Lerdahl, P.E. Øren, S. Bakke, in: Proceedings of the SPE/DOE Conference on Improved Oil Recovery, Tulsa, OK, 2000, SPE59311.
[26] M. Sohrabi, G. Henderson, D.H. Tehrani, A. Danesh, in: Proceedings of the SPE Annual Technical Conference and Exhibition, Dallas, TX, 2000, SPE63000.
[27] M. Sohrabi, D.H. Tehrani, A. Danesh, G. Henderson, in: Proceedings of the SPE Annual Technical Conference and Exhibition, New Orleans, 2001, SPE71494.
[28] J.S. Rowlinson, B. Widom, Molecular Theory of Capillarity, Clarendon Press, Oxford, 1989.
[29] F.E. Bartell, H.J. Osterhof, Ind. Eng. Chem. 19 (1927) 1277–1280.
[30] A.A. Keller, M.J. Blunt, P.V. Roberts, Transport Porous Media 26 (1997) 277–297.
[31] M.I.J. van Dijke, K.S. Sorbie, S.R. McDougall, Adv. Water Resources 24 (2001) 365–384.
[32] M.I.J. van Dijke, K.S. Sorbie, J. Petrol. Sci. Eng. 33 (2002) 39–48.
[33] N.R. Morrow, F. McCaffery, in: G.F. Padday (Ed.), Wetting, Spreading, and Adhesion, Academic Press, New York, 1978, pp. 289–319.